

Method for Accurate Surface Temperature Measurements During Fast Induction Heating

Benjamin Larregain, Nicolas Vanderesse, Florent Bridier, Philippe Bocher, and Patrick Arkinson

(Submitted June 25, 2012; published online April 13, 2013)

A robust method is proposed for the measurement of surface temperature fields during induction heating. It is based on the original coupling of temperature-indicating lacquers and a high-speed camera system. Image analysis tools have been implemented to automatically extract the temporal evolution of isotherms. This method was applied to the fast induction treatment of a 4340 steel spur gear, allowing the full history of surface isotherms to be accurately documented for a sequential heating, i.e., a medium frequency pre-heating followed by a high frequency final heating. Three isotherms, i.e., 704, 816, and 927°C, were acquired every 0.3 ms with a spatial resolution of 0.04 mm per pixel. The information provided by the method is described and discussed. Finally, the transformation temperature A_{c1} is linked to the temperature on specific locations of the gear tooth.

Keywords 4340 steel gear, induction heating, temperature measurement

1. Introduction

As a green manufacturing process, induction heating has become a very interesting alternative for the contour hardening of gears in the aeronautical industry, in replacement of the currently used thermochemical processes. Induction contour hardening equipments are designed to locally harden a part with a coil using medium (MF) and/or high frequency (HF) generators. The depth of the hardened layer depends on numerous factors, including the induction heating parameters, the workpiece geometry, and the material metallurgical and physical properties (Ref 1). Even if the use of designs of experiments (Ref 2) can provide pertinent results to develop a specific treatment, it remains time consuming and costly as the parts are already in an advanced manufacturing state before the surface hardening stage. Consequently, the development of computer simulation tools is required to allow designers to develop and optimize induction processes more efficiently. Complex multiphysical numerical approaches have to be used due the nature of the process encompassing electro-magnetic, thermal, metallurgical, and mechanical phenomena (Ref 3). The final state, after both induction heating and quenching phases,

is usually considered for the validation of the numerical simulations. Little or no transient information is taken into account. Four final responses can be typically used, i.e., the hardness profile, the microstructure transformation, the residual stresses profile, and the level of distortions. However, the microstructure gradient and the residual stresses' profile are typical features which depend on the thermal path of the heated and quenched part. Getting accurate information on the temperature field evolution versus time within an induction heated part is a critical way to not only validate the numerical models but also optimize the process itself (Ref 4).

However, the measurement of temperature evolution during induction heating faces several issues. First, the austenitic transformation temperatures of usual hardened steels are between 750 and 1000°C. The temperature measurement technique employed must be able to provide data from ambient temperature to these high temperature levels. On the other hand, current induction heating processes use powerful generators able to heat the part in a fraction of a second (Ref 5-7) and the measurement medium must provide very high acquisition rates, i.e., a HF of signal acquisition and the shorter response time possible. Finally, the thermal gradients may be highly localized and there is a need to have a high spatial resolution for the measurement.

Four temperature measurement methods were tested. Table 1 summarizes their characteristics relative to the induction heating application, i.e., the allowed temperature range, the location, and the accuracy the temperature measurement provided by each method.

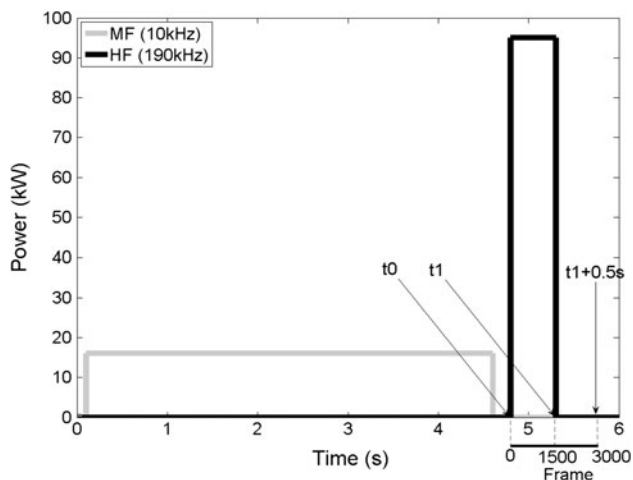
The impossibility of temperature measurement during a rotating movement, which is common in induction heating of spur gear, is a major inconvenience of thermocouples. Moreover, thermocouples only provide information on local temperature and also impose a compromise between maximal allowed temperature and acquisition speed. For a local measurement at a 0.5-mm-diameter spot, the pyrometer is a good alternative, but its accuracy strongly depends on the calibration of the material emissivity which evolves with temperature and the environment reflectivity. For a surface measurement, an alternative is the

This article is an invited paper selected from presentations at the 26th ASM Heat Treating Society Conference, held October 31 through November 2, 2011, in Cincinnati, OH, and has been expanded from the original presentation.

Benjamin Larregain, Nicolas Vanderesse, Florent Bridier, and Philippe Bocher, Mechanical Engineering Department, École de Technologie Supérieure, Montreal, QC, Canada; and **Patrick Arkinson**, Pratt & Whitney Canada, Longueuil, QC, Canada. Contact e-mail: Benjamin.Larregain@etsmtl.ca.

Table 1 Characteristics of temperature measurements means in the context of induction heating

| | Range and area | Accuracy |
|---------------------------------|---|--|
| Thermocouple (K-type) | [0-1250°C] A spot on the surface or within the part | ≈0.5-4 s of response time 2.2°C or 2% of the temperature |
| Infrared pyrometer | [0-1650°C] 0.5-mm-diameter spot on the surface | ±1% of the temperature ≈10-100 ms of response time |
| Infrared camera | [0-1200°C] Full-field surface | ±1% of the temperature ≈10-100 ms of response time |
| Temperature-indicating lacquers | Discrete values from 25 to 1050°C Full-field surface | ±1% of the indicated temperature ≈1 ms of response time |

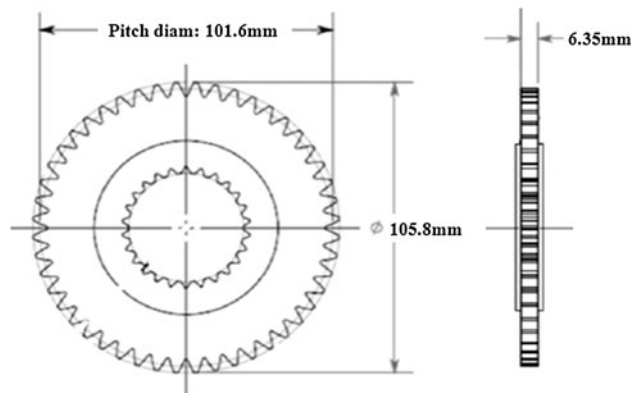
**Fig. 1** Induction heating process parameters

full-field infrared camera measurement, but this technique is also very sensitive to the material emissivity versus its temperature. Furthermore, concerning these three temperature measurement media, the response time and acquisition frequency of the data logger have to be added to the tool response time, providing long system response times. On the other hand, temperature-indicating lacquers are usually used as a static measurement to localize where a temperature has been reached or not at the surface of a part.

The method developed in the present work consists of filming at a high speed rate gear teeth covered with different temperature-indicating lacquers. It allows a direct and full-field measure of the corresponding isotherm during the induction heating. From the acquisition and analysis of three different isotherms during the induction heating of a spur gear, a range of the Ac1 transformation temperatures will be defined versus the local heating rate at the gear tooth surface and compared with literature data.

2. Experimental Procedure

The induction heating treatments were performed using a single-turn coil on a dual simultaneous MF and HF frequencies' generator designed by EFD Induction Sa. The coil had a 110-mm inner diameter and a 6 mm thickness. The heating procedure consisted of a 4.5-s MF preheating followed by a 0.5-s HF heating and a final air cooling (Fig. 1) without rotating the gear. The times t_0 and t_1 correspond to the beginning and the end of the HF heating phase. The hardened

**Fig. 2** Spur gear geometry

Spur gear data (heat-treated part)

| | |
|---------------------|----------------|
| Number of teeth | 48 |
| Diametral pitch | 12.00 |
| Pressure angle | 25.00° |
| Outside diameter | 105.84 mm |
| Base diameter | 92.08 mm |
| Root diameter | 95.38-95.50 mm |
| Pitch diameter | 101.6 mm |
| Form diameter | 97.88 mm |
| Arc tooth thickness | 3.20-3.25 mm |
| Tooth length | 6.35 mm |

spur gear is made of quenched and tempered SAE 4340 martensitic steel. The gear's geometry is described in Fig. 2.

The experimental setting is shown in Fig. 3. Prior to each test, the upper side of the spur gear was coated with a specific temperature-indicating lacquer. Such lacquers contain chemicals in suspension that transform or evaporate at given temperatures, with an accuracy of ±1% of the indicated temperature. A high-speed camera is set 25 cm above the gear by means of a tripod. The magnification is adjusted so that two teeth are observed within the camera's field of view. The gear is lightened up enough for the lacquer coating to appear uniform. The camera records 512×352 pixels images at a frame rate of 3000 images per second. A total duration of 4 s (12,000 images) is recorded for each test. The resulting images have a spatial resolution of $40 \mu\text{m}/\text{pixel}$ and a temporal resolution of 0.3 ms between two frames. A typical image is shown in Fig. 4.

The interface between the evaporated and the non-evaporated lacquer indicates the isotherm specific to this lacquer. The goal of a test is then to determine the exact location of this

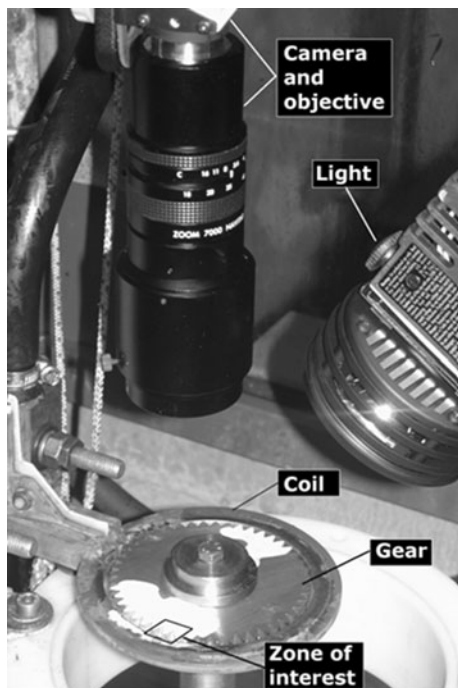


Fig. 3 Experimental setting

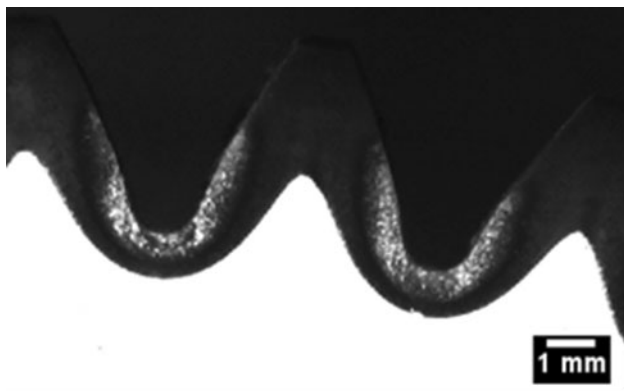


Fig. 4 Example of an image recorded during HF heating

curve and follow this location during the heating phase. In order to automatically perform the data treatment, image analysis operations have been implemented and carried out using either the free software Fiji, based on ImageJ (Ref 8), or the image-processing toolbox of Matlab®.

The different steps required for extracting an isotherm from the raw images recorded by the camera system are summarized in Fig. 5, where the following convention, derived from object-oriented programming, is used: A rectangle stands for an image or a group of images and an oval stands for an operation. An operation takes one or several images as input and returns one or several images as output. Operations and images are related by arrows. An arrow pointing from an image to an operation means that the image is used as an input by the operation, while an arrow pointing from an operation to an image identifies the image as the output of the operation. Only the main output/input images are indicated, along with references to corresponding figures.

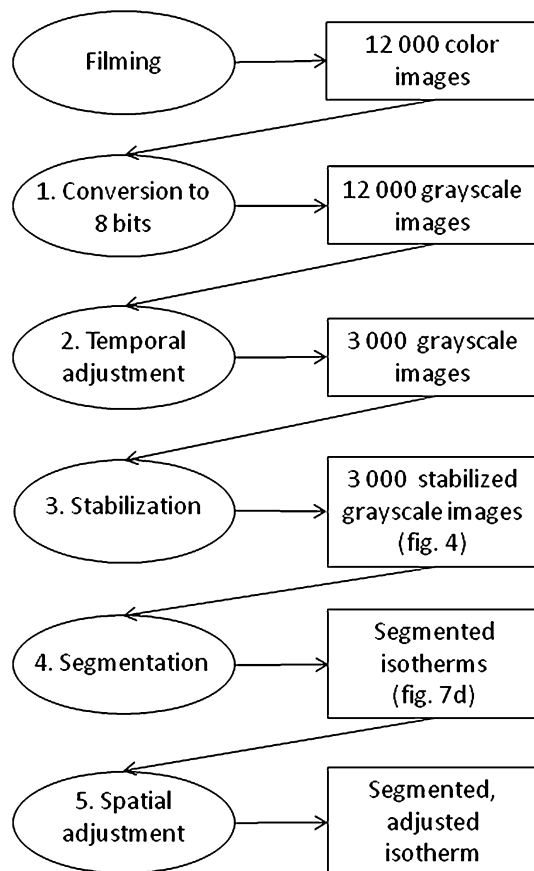


Fig. 5 Image-processing operations for all images corresponding to one heat treatment. The segmentation step is detailed in Fig. 6

2.1 Conversion to Gray

The 12,000 images composing the movie are first converted into 8-bit images (255 gray levels).

2.2 Temporal Adjustment

This operation aims at synchronizing all tests with each other. Indeed, a test is limited to the determination of a single isotherm. The reproducibility of the heating of each of these tests has been thoroughly verified. In order to fully assess the temperature evolution of the part, it is necessary to gather all isotherms within a single, common temporal frame. Images taken for different isotherms, i.e., during different but fully identical tests, are not synchronized. A temporal adjustment is thus needed. It is carried out at the beginning of the treatments and consists of defining a timing reference to which all tests will be referred. By convention, this temporal reference is defined as the end of the HF heating treatment. It is automatically determined by identifying the frame in which the intensity at the root between the teeth is maximal. 1500 images before this moment and 1500 images after are then selected. This yields a time span of 3000 images (i.e., 1 s) that covers the 0.5-s HF heating treatment and the following air cooling for each test.

2.3 Stabilization

The stabilization operation intends to eliminate the vibrations which introduce small periodic translations between successive images. An implementation of the Lukas-Kanade algorithm for ImageJ is used for this task (Ref 9).

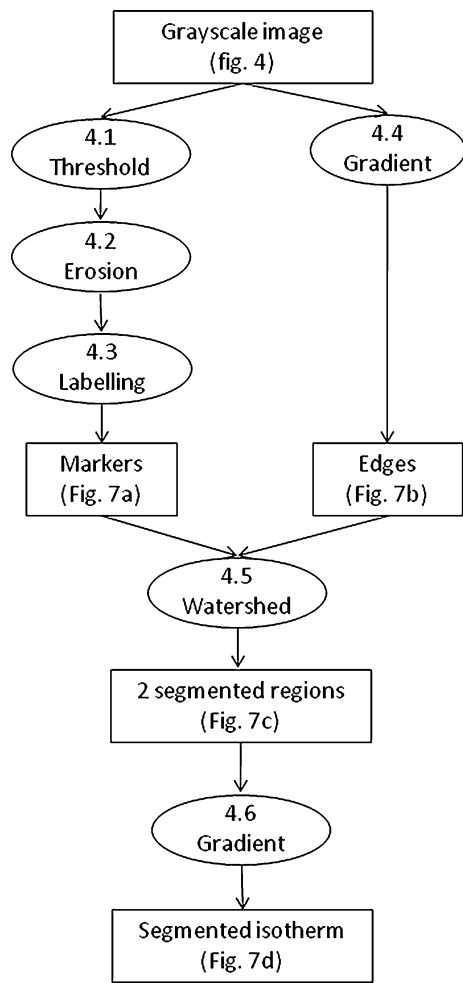


Fig. 6 Image segmentation operations for a single image

2.4 Segmentation

The goal of the segmentation step is to divide each image into two regions, namely the non-evaporated lacquer and the rest of the image. This step involves distinct sub-operations described in Fig. 6. Choosing a reliable strategy of segmentation adapted to the images and to the information that must be derived from them is a general issue in image processing. In this work, a simple threshold could be considered, i.e., a transformation which assigns the maximal value to bright pixels above a given value and sets the others the minimal value. Nevertheless, such a method is actually error prone since the intensity of successive images may undergo global and local variations due to external perturbations such as, for the present experiments, the smoke produced by evaporation of lacquers or the light emitted by the material at high temperatures. A more robust approach is needed. While there exists no general solution for efficiently segmenting any given type of image, a so-called “marker-controlled watershed” on the initial image or its gradient proves to be reliable in most cases (Ref 10). This approach is considered as the general paradigm proposed by mathematical morphology. The principle of the watershed relies on the equivalence between a gray valued image and a topographic surface, each gray level corresponding to a certain height. The surface can be described in terms of hills and basins that visually relate to bright and dark zones,

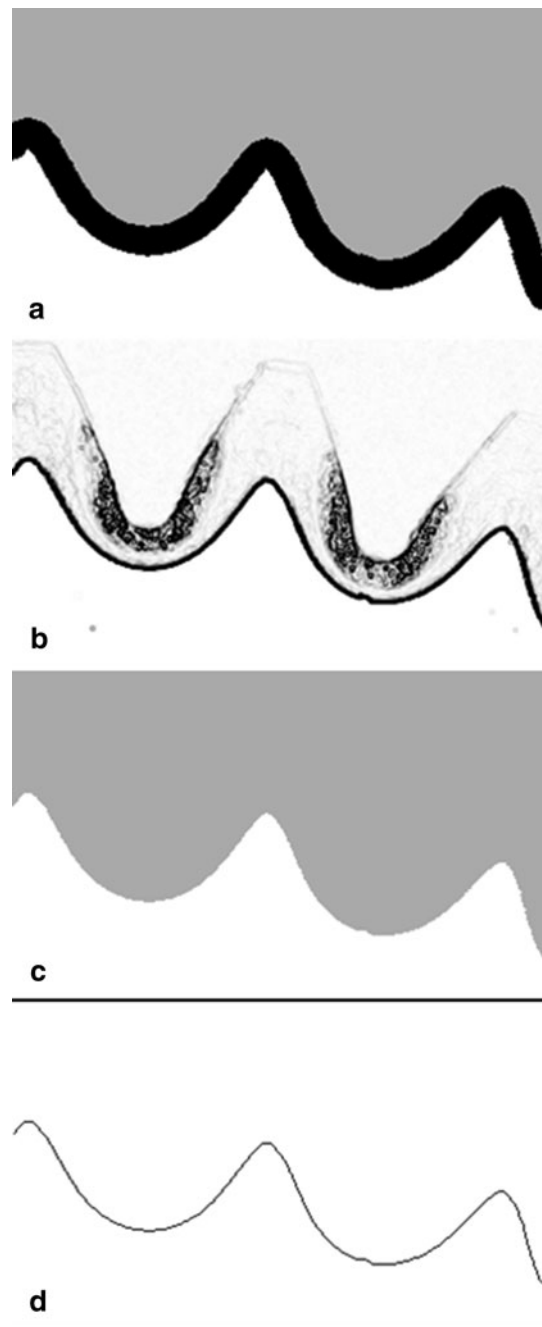


Fig. 7 Images corresponding to different steps in the image processing of Fig. 4. (a) Markers, (b) gradient, (c) watershed output, and (d) isotherm

respectively. The watershed operation consists of identifying the basins by determining the positions of the ridges that separate them. Each basin thus corresponds to a region that will be segmented. The interested reader is referred to Ref 11 and 12 for an in-depth description of this operation.

In the marker-controlled version of the algorithm, only basins identified by so-called *markers* are taken into account, the others being ignored. Visually, the markers are represented by homogeneous zones, each identified by a distinctive gray level. They are separated by black layers which indicate the approximate location of the ridges between the basins. Two main steps are thus required: First, the different regions to be segmented must be identified by markers (operations 4.1-4.3 in

Fig. 6); second, the markers are used with the original image or its gradient (operation 4.4) by the watershed algorithm itself (operation 4.5).

4.1, 4.2, 4.3. *Threshold, Erosion, and Labeling* There are various ways to create markers from an image. In this work, they are derived from a threshold of the original image. Two markers are created, one for the intact lacquer, the other one for the evaporated lacquer and the exterior of the part. They appear as two complementary regions that cover the whole image. They then must be separated by a black layer that approximately locates the position of the border between the regions to be segmented. The black layer is created by grayscale erosion which reduces the surface covered by non-zero pixels. The markers are then each assigned a distinct gray level (labeling operation). The resulting image is shown in Fig. 7(a).

4.4. *Gradient of the Original Image* The gradient, or spatial derivative, highlights the edges between the different homogeneous zones of the original image and thus facilitates the detection of ridges (Fig. 7b, inverted for the ease of visualization).

4.5. *Marker-Controlled Watershed* The image of the markers is then used in combination with the gradient of the initial image (Fig. 7b) by the watershed algorithm. The output is an image composed of two complementary regions (Fig. 7c).

4.6. *Gradient of the Segmented Image* The isotherm is determined by computing the border between both regions (Fig. 7d).

2.5 Spatial Adjustment

In spite of the care given to the experimental setting, the images produced by different tests may have slightly different orientations and dimensions. The last step consists of the spatial adjustment of the batch of segmented images in order to have a common spatial reference frame for all isotherms issued from different tests. This is achieved by a series of rotations, rescaling, and translations. For illustration purposes, the final isotherm is superimposed on the original image in Fig. 8, where the original image has been slightly darkened for the ease of visualization.

3. Results

A full characterization of the temperature evolution versus time has been conducted at the surface of two teeth of the gear heated by MF preheating and 0.5-s HF heating and then cooling

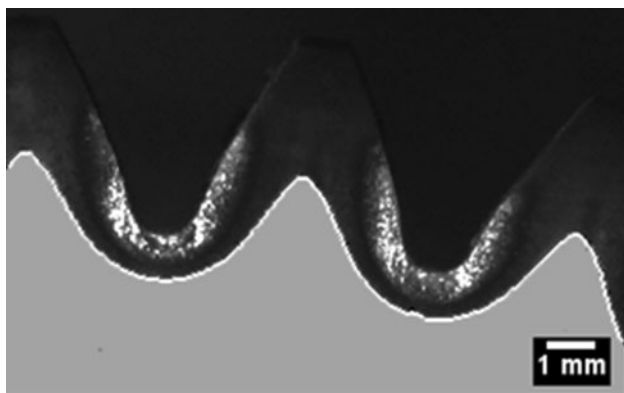


Fig.8 Overlay of the isotherm in Fig. 7(d) and the original image in Fig. 4

in air. Three isotherms, i.e., 704, 816, and 927°C, are depicted in Fig. 9 for different times of the HF heating phase.

A qualitative analysis of the HF heating phase highlights the fact that the temperature rises first at the tooth root and then at the tip due to the temperature initial state of the surface after the MF preheating phase. Indeed, during the MF preheating phase, Eddy currents are concentrated at the tooth root and the resulting Joule effect makes the gear more heated in this area. Consequently, despite the fact that HF heating is known to heat the nearest parts of the tooth to the coil, i.e., the tooth tip, the present method allowed the original identification of three heating steps of temperature evolution during HF heating: temperature increases first at the tooth root, then along the edge of the active profile, and finally in the rest of the tooth surface. Note that the evaporation of the temperature-indicating lacquers is by nature non-reversible. It is then only possible to document if a point at the surface reached a certain temperature at a certain time. Therefore, if potential temperature diffusion can be documented during the cooling phase, any temperature decrease cannot be characterized. During the air cooling phase of the present experiment, isotherms slightly evolved during 0.1 s after the HF heating phase and did not evolve anymore

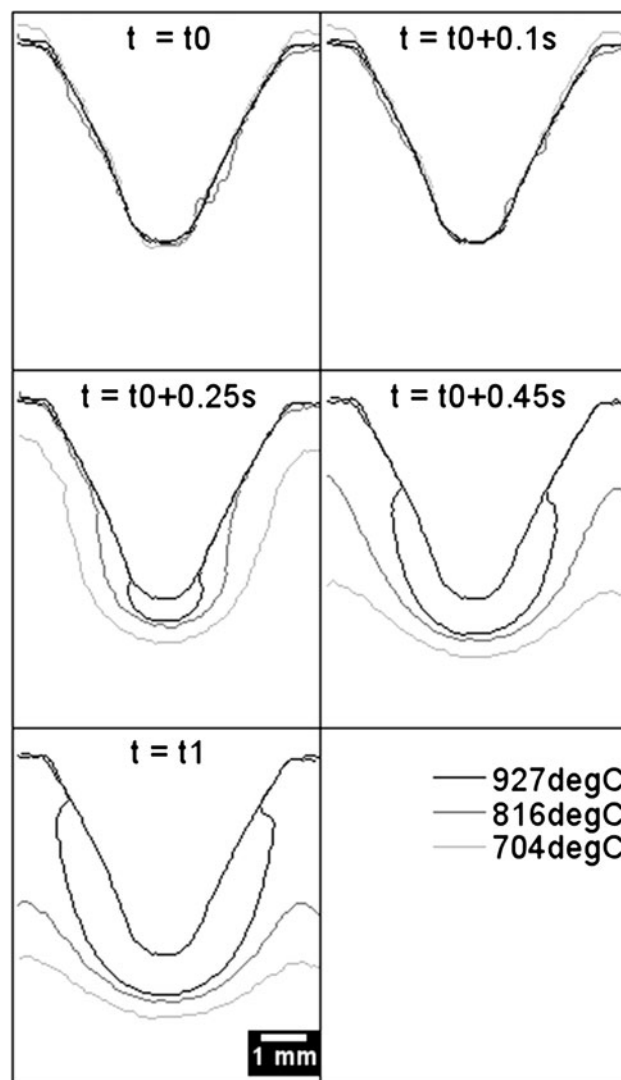


Fig. 9 Isotherms at five steps from the beginning to the end of the HF heating

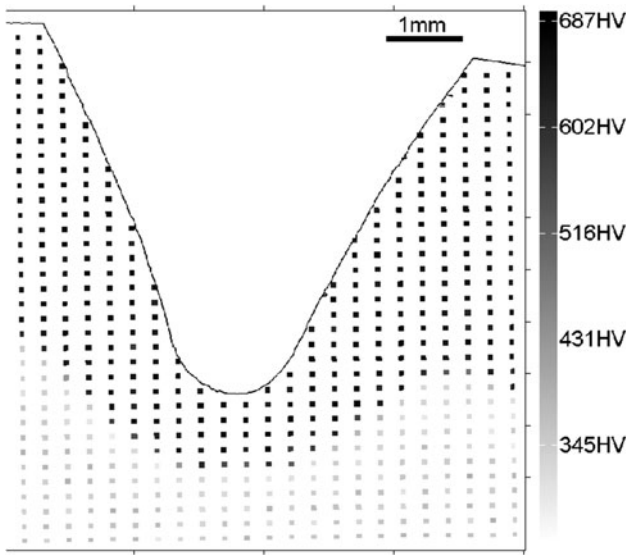


Fig. 10 Hardness results

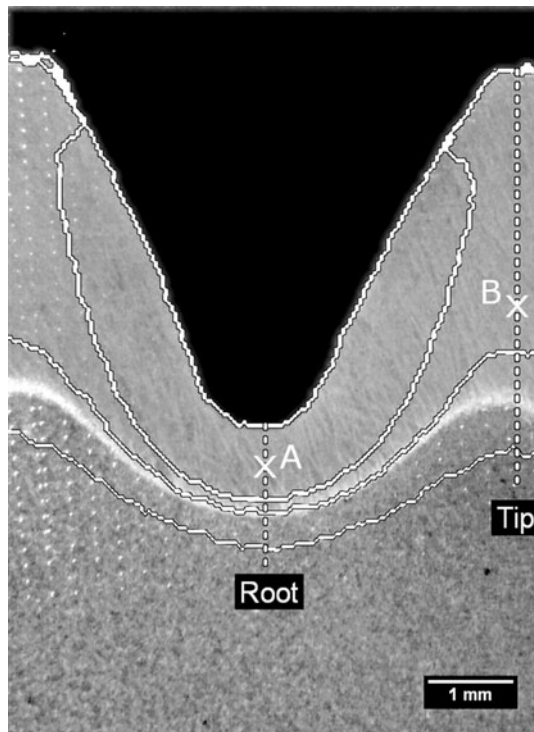


Fig. 11 Overlay of the etched microstructure with isotherms at 927, 816, and 704°C (white lines, from top to bottom). The dashed lines correspond to profiles presented in Fig. 12

after. Therefore, very little temperature diffusion is observed at the surface of the gear after the end of induction heating.

According to the ASTM E384-99 standard, local microhardness measurements were automatically performed on the whole tooth surface with a 300-g load during 13 s. The grid of microhardness indents is defined by a 0.2-mm step in the vertical direction and a 0.3-mm step in the horizontal direction. As shown in Fig. 10, the tooth surface hardness is clearly defined by a hardened layer around 685 HV and a core hardness around 350 HV.

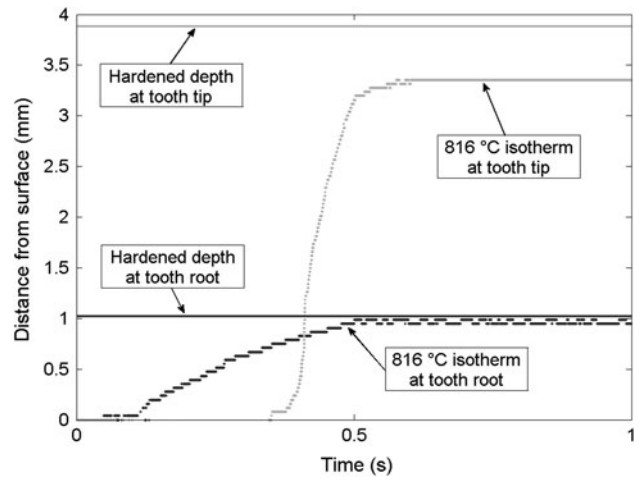


Fig. 12 Temporal profiles of the 816°C isotherm at the root and tip of a tooth (white dashed lines in Fig. 11)

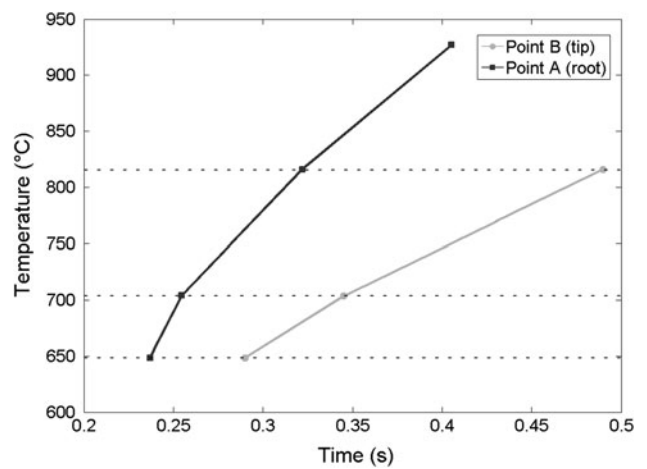


Fig. 13 Temperature vs. time at points A (root) and B (tip) in Fig. 11

The etched microstructure, the result of the induction hardening and air cooling, is also shown in Fig. 11. It can be observed that the hardened layer and the core are separated by a brighter line area corresponding to the transition zone. The final isotherms' positions are superimposed with the etched microstructure in order to locate the interface between hardened and non-hardened regions relative to them. The comparison of the distances between the transition line and the isotherms makes it possible to evaluate the transformation temperature locally. The evolution of the 816°C isotherm is also plotted versus time in Fig. 12 for the tooth root and the tooth tip and compared with the hardened depths at these two locations.

As shown in Fig. 11 and 12, at the tooth root, the hardened depth corresponds to the final position reached by the 816°C isotherm, whereas it corresponds to a temperature included into the range 704-816°C at the tooth tip. Thus, the hardness frontier may not be associated with a single isotherm. This result can either suggest very different temperature gradients or that the material experienced different transformation temperatures at different locations of the tooth. This latter is thought by the authors to be more plausible since transformation phenomena are known to be not only temperature dependent but also heating rate dependent (Ref 13-15). From the measurements

obtained via the present method, the temperature rate can actually be estimated by plotting the evolution of temperature versus time. In Fig. 13, temperature evolution is given at two arbitrary points within the hardened layer, one located at 0.72 mm from the root and the other one at 3.12 mm from the tip (points A and B in Fig. 11, respectively). The result is shown in Fig. 13. It can be observed that the heating rate is much higher at the tooth root than at the tooth tip, i.e., 1650 and 835°C/s, respectively. This significant difference could result in a higher Ac1 at the tooth root than at the tooth tip. This trend is in agreement with the results of Ref 13-15.

4. Conclusions

A method for full-field surface temperature measurement during fast heating conditions has been developed. It makes use of a high-speed camera system combined with temperature-indicating lacquers. In this work, a spatial resolution of 0.04 mm/pixel and a temporal resolution of 0.3 ms between two images were achieved. The thermal history at the side of a spur gear during HF heating was accurately measured by means of an image analysis procedure. In particular, one can document where and when a given temperature is reached at the surface of a whole gear tooth hardened by fast induction heating.

The final position of isotherms was compared to the hardness transition line. The results suggest that the transformation temperature Ac1 varied with the position at the surface of the part. The heating rates were estimated at two locations, showing that the temperature at the root increased faster than at the tip. This method thus allowed confirming the correlation between the Ac1 temperature and the heating rate.

Further work shall focus on determining more isotherms in order to accurately evaluate the variation of Ac1 at very high heating rates. The full history of surface isotherms will also be studied for different heating parameters, i.e., with or without preheating, through either simultaneous or sequential HF/MF final heating. Finally, such temperature data can be of great interest for validation or calibration of computer simulations of induction heating.

References

1. J. Grum, Induction Hardening, *Handbook of Residual Stress and Deformation of Steel*, G. Totten, M. Howes, and T. Inoue, Ed., ASM International, New York, 2002, p 220–223
2. H. Kristoffersen and P. Vomacka, Influence of Process Parameters for Induction Hardening on Residual Stresses, *Mater. Des.*, 2001, **22**(8), p 637–644
3. V. Nemkov, Modeling of Induction Hardening Processes, *Handbook of Thermal process Modeling Steels*, C.H. Gür and J. Pan, Ed., Taylor & Francis Group, New York, 2008, p 428–431
4. V. Rudnev et al., *Handbook of Induction Heating*, Taylor & Francis Group, New York, 2002
5. Y. Misaka, Y. Kiyosawa, K. Kawasaki, T. Yamazaki, and W.O. Silverthorne, *Gear Contour Hardening by Micropulse Induction Heating System*, S.o.A. Engineers, Ed., 1997, p 121–130
6. J. Komotori et al., Fatigue Strength and Fracture Mechanism of Steel Modified by Super-Rapid Induction Heating and Quenching, *Int. J. Fatigue*, 2001, **23**(1), p 225–230
7. T. Inoue, et al., Simulation of Dual Frequency Induction Hardening Process of a Gear Wheel, *3rd International Conference on Quenching and Control of Distortion* (Prague, Czech Republic), 1999, p 243–250
8. M.D. Abramoff, P.J. Magelhaes, and S.J. Ram, Image Processing with ImageJ, *Biophotonics Int.*, 2004, **11**(7), p 36–44
9. K. Li and S. Kang, *The Image Stabilizer Plugin for ImageJ*, 2008, Last Accessed 18 May 2011 from http://www.cs.cmu.edu/~kangli/code/Image_Stabilizer.html
10. S. Beucher and F. Meyer, The Morphological Approach of Segmentation: The Watershed Transformation, *Mathematical Morphology in Image Processing*, E. Dougherty, Ed., Marcel Dekker, New York, 1992, p 433–481
11. S. Beucher, Mathematical Morphology and Geology: When Image Analysis Uses the Vocabulary of Earth Science: A Review of Some Applications, *International Symposium on Imaging Applications in Geology*, D. Jongmans, E. Pirard, and P. Trefois, Ed., Université de Liège, Liège, 1999, p 13–16
12. J.B.T.M. Roerdink and A. Meijster, The Watershed Transform: Definitions, Algorithms, and Parallelization Strategies, *Fundam. Inform.*, 2001, **41**, p 187–228
13. V. Rudnev, *Be Aware of the 'Fine Print' in the Science of Metallurgy of Induction Hardening*, Industrial Heating, 2005, p 1–5
14. W.J. Feuerstein and W.K. Smith, Elevation of Critical Temperatures in Steels by High Heating Rates, *Trans. ASM*, 1953, **46**, p 1271–1284
15. K. Clarke et al., Induction Hardening 5150 Steel: Effects of Initial Microstructure and Heating Rate, *J. Mater. Eng. Perform.*, 2011, **20**(2), p 161–168